Journal of Alzheimer's Disease 51 (2016) 1045–1056
DOI 10.3233/JAD-151010
IOS Press

Prediction of Progressive Mild Cognitive Impairment by Multi-Modal Neuroimaging Biomarkers

Lele Xu[a], Xia Wu[a,b,*], Rui Li[c], Kewei Chen[d], Zhiying Long[b], Jiacai Zhang[a], Xiaojuan Guo[a] and Li Yao[a,b] and for the Alzheimer's Disease Neuroimaging Initiative[1]
[a]*College of Information Science and Technology, Beijing Normal University, Beijing, China*
[b]*State Key Laboratory of Cognitive Neuroscience and Learning & IDG/McGovern Institute for Brain Research, Beijing Normal University, Beijing, China*
[c]*Center on Aging Psychology, Key Laboratory of Mental Health, Institute of Psychology, Chinese Academy of Sciences, Beijing, China*
[d]*Banner Alzheimer's Institute and Banner Good Samaritan PET Center, Phoenix, AZ, USA*

Accepted 4 January 2016

Abstract. For patients with mild cognitive impairment (MCI), the likelihood of progression to probable Alzheimer's disease (AD) is important not only for individual patient care, but also for the identification of participants in clinical trial, so as to provide early interventions. Biomarkers based on various neuroimaging modalities could offer complementary information regarding different aspects of disease progression. The current study adopted a weighted multi-modality sparse representation-based classification method to combine data from the Alzheimer's Disease Neuroimaging Initiative (ADNI) database, from three imaging modalities: Volumetric magnetic resonance imaging (MRI), fluorodeoxyglucose (FDG) positron emission tomography (PET), and florbetapir PET. We included 117 normal controls (NC) and 110 MCI patients, 27 of whom progressed to AD within 36 months (pMCI), while the remaining 83 remained stable (sMCI) over the same time period. Modality-specific biomarkers were identified to distinguish MCI from NC and to predict pMCI among MCI. These included the hippocampus, amygdala, middle temporal and inferior temporal regions for MRI, the posterior cingulum, precentral, and postcentral regions for FDG-PET, and the hippocampus, amygdala, and putamen for florbetapir PET. Results indicated that FDG-PET may be a more effective modality in discriminating MCI from NC and in predicting pMCI than florbetapir PET and MRI. Combining modality-specific sensitive biomarkers from the three modalities boosted the discrimination accuracy of MCI from NC (76.7%) and the prediction accuracy of pMCI (82.5%) when compared with the best single-modality results (73.6% for MCI and 75.6% for pMCI with FDG-PET).

Keywords: Florbetapir positron emission tomography, fluorodeoxyglucose positron emission tomography, magnetic resonance imaging, mild cognitive impairment, multi-modality, prediction, progressive mild cognitive impairment

[1]Data used in preparation of this article were obtained from the Alzheimer's Disease Neuroimaging Initiative (ADNI) database (http://adni.loni.usc.edu). As such, the investigators within the ADNI contributed to the design and implementation of ADNI and/or provided data but did not participate in analysis or writing of this report. A complete listing of ADNI investigators can be found at: http://adni.loni.usc.edu/wp-content/uploads/how_to_apply/ADNI_Acknowledgement_List.pdf.

*Correspondence to: Xia Wu, College of Information Science and Technology, Beijing Normal University, No. 19 Xin Jie Kou Wai Da Jie, Beijing 100875, China. Tel./Fax: +86 010 58800441; E-mail: wuxia@bnu.edu.cn.

INTRODUCTION

Mild cognitive impairment (MCI) has been suggested as the precursor stage of Alzheimer's disease (AD) because of the probable conversion to AD [1, 2]. Over time, some MCI patients convert to AD (denoted as progressive MCI, pMCI), while others remain stable or even revert to normal healthy cognitive status (defined as stable MCI, sMCI) [3]. The accurate prediction of MCI, especially pMCI that probably converts to AD, is significant for the timely provision of patient care.

Besides the criteria of the National Institute of Neurological and Communicative Disorders and Stroke/Alzheimer's Disease and Related Disorders Association (NINCDS/ADRDA) [4], biomarkers from various neuroimaging modalities have been increasingly suggested as of utility in predicting MCI and pMCI [5–8]. Such biomarkers include those obtained from volumetric magnetic resonance imaging (MRI) and positron emission tomography (PET) measuring either metabolic or pathological burden using different radioactive tracers.

Volumetric MRI measures have been widely used to detect the structural changes in the early stage of AD (e.g., MCI) [9–13]. For example, Jefferson et al. used hippocampal volume and cortical thickness to predict MCI conversion [9]; Fan et al. considered spatial patterns of brain atrophy including the hippocampus, medial temporal lobe, orbitofrontal, and medial prefrontal grey matter to identify MCI patients [10]; Zhang et al. identified regional gray matter volumes in the hippocampus, amygdala, and thalamus to predict the cognitive impairment of MCI patients [11]; Willette et al. performed independent component analysis on gray matter images and used several independent components to diagnose MCI [12]; Risacher et al. revealed that besides decreased hippocampal volume being a robust biomarker to predict MCI, the medial temporal structure was also a promising MRI marker for the same purpose [13].

Fluorodeoxyglucose PET (FDG-PET), which measures cerebral glucose metabolism, provides sensitive biomarkers for the prediction of MCI and converters [14–16]. For instance, Mosconi et al. reported that hypometabolism in the inferior parietal cortex was indicative of potential MCI progression [14]; Chen et al. revealed that the hypometabolic convergence index based on FGD-PET could be applied to distinguish those who progressed to AD from those who did not among patients with MCI [15]; Cerami et al. found hypometabolism in the orbitofrontal region, anterior cingulate cortex, and temporal lobe in patients with MCI [16].

Most recently, florbetapir PET, which measures the accumulation of amyloid in the brain, has been introduced to study MCI [17, 18]. For example, Camus et al. reported that patients with MCI showed a relatively high uptake of florbetapir in the posterior cingulate cortex [17]; Rosenberg et al. found that greater standardized uptake value ratios (SUVR) were associated with poorer performance on all cognitive tests; the averaged SUVR of occipital, parietal, precuneus, temporal, and anterior cingulate regions were correlated with cognition scores, such as the Alzheimer's Disease Assessment Scale-Cognitive subscale (ADAS-Cog) [18].

The biomarkers from different neuroimaging modalities could reflect different aspects of the early stages of diseases. Combination of biomarkers from different imaging modalities could offer complementary information for a given disease [19–22] and might facilitate more accurate diagnosis or prediction results than single-modality biomarkers [5, 23, 24]. Multiple studies have reported a combination of different modalities in investigating MCI. For example, when combining MRI and cerebrospinal fluid (CSF) data [5, 25, 26], Westman et al. achieved an accuracy of 77.6% in classifying MCI from normal controls (NC), which was superior to each of the single-modality results (71.8% for MRI and 70.3% for CSF). Furthermore, adopting MRI + CSF they also predicted the conversion from MCI to AD within 36 months with an accuracy of 66.1% [5]; Regarding MRI and FDG-PET [21–23], Liu et al. combined these modalities in discriminating MCI from NC and achieved better performance than using single-modality biomarkers [23]; When combining MRI, CSF, and FDG-PET [24, 27], Zhang et al. discriminated MCI from NC with an accuracy of 76.4%, which was again superior to the single-modality results (72.0% for MRI, 71.4% for CSF, and 71.6% for FDG-PET) [24].

In this study, we explored the contribution of different neuroimaging modalities in their predictive power and characterized the sensitive biomarkers from each modality, so as to conveniently and effectively predict MCI/pMCI. We used data from the Alzheimer's Disease Neuroimaging Initiative (ADNI) database encompassing three modalities: MRI, FDG-PET, and florbetapir PET. A multi-modal algorithm based on sparse representation-based classification (wmSRC) [28] was applied to study the baseline differences between MCI and NC and between pMCI (who

converted to AD within 36 months) and sMCI (who did not convert to AD within 36 months). The experimental results indicated that FDG-PET may contribute more to the accurate prediction of MCI/pMCI than florbetapir PET when using a set of brain regions as features. Furthermore, the results also suggested that combining features from MRI, FDG-PET, and florbetapir PET increases the accuracy of discriminating MCI from pMCI, compared with using features from a single-modality; a small set of modality-specific sensitive biomarkers were identified for effectively predicting MCI/pMCI.

MATERIALS AND METHODS

Participants

Data used in the preparation of this article were obtained from the ADNI database (http://adni.loni.usc.edu). The ADNI was launched in 2003 as a public-private partnership, led by principal investigator Michael W. Weiner. The primary goal of ADNI has been to test whether serial MRI, PET, other biological markers, and clinical and neuropsychological assessments can be combined to measure the progression of MCI and early AD. The determination of sensitive and specific markers for very early AD progression is intended to aid researchers and clinicians in developing new treatments and monitoring their effectiveness and lessening the time and cost of clinical trials. ADNI is the result of the efforts of many co-investigators from a broad range of academic institutions and private corporations, and subjects have been recruited from over 50 sites across the United States and Canada. The initial goal of ADNI was to recruit 800 adults, aged 55 to 90 years, to participate in the study (approximately 200 cognitively normal older individuals to be followed for 3 years, 400 people with MCI to be followed for 3 years, and 200 people with early AD to be followed for 2 years). The research protocol was approved by the institutional review board of each participating site and written informed consent was obtained from each participant. For up-to-date information, see http://www.adni-info.org.

Three imaging modalities were investigated, namely MRI, FDG-PET, and florbetapir PET, and a total of 227 subjects were included, consisting of 110 patients with MCI (27 cases of pMCI, which converted to AD within 36 months; and 83 cases of sMCI, which remained stable during the same time interval, or the participant left the study) and 117 NC subjects. The subjects were between 55 and 90 years old. The Mini-Mental State Examination (MMSE) [29] and Clinical Dementia Rating (CDR) scores [30] were used to assess the severity of cognitive impairment according to ADNI protocols. General inclusion/exclusion criteria were as follows: 1) MCI subjects: MMSE scores between 24 and 30 (inclusive), subjective memory complaints, objective memory loss measured by education-adjusted scores on the Wechsler Memory Scale Logical Memory II [31], a CDR of 0.5, absence of significant levels of impairment in other cognitive domains, essentially preserved activities of daily living, and an absence of dementia; 2) NC subjects: MMSE scores between 24 and 30 (inclusive), a CDR of 0, non-depressed, without MCI, and non-demented. The clinical and demographic information are listed in Table 1, and the IDs of each participant in the ADNI dataset are shown in Supplementary Table 1.

Table 1
The clinical and demographic characteristics of the subjects that included in this study, the *p*-value is obtained by one-way ANOVA over the pMCI, sMCI, and NC groups

	pMCI	sMCI	NC	*p*-value
Gender	14M/13F	45M/38F	62M/55F	0.97
Age	74.0 ± 7.6	75.7 ± 7.9	75.4 ± 7.0	0.57
MMSE	26.5 ± 1.9	27.7 ± 1.8	28.9 ± 1.3	1.48e-12
CDR	0.5 ± 0.0	0.5 ± 0.0	0.0 ± 0.0	<1e-100

pMCI, progressive mild cognitive impairment; sMCI, stable mild cognitive impairment; NC, normal control; M, male, F, female; MMSE, Mini-Mental State Examination; CDR, Clinical Dementia Rating.

Data preprocessing

All the MRI, FDG-PET, and florbetapir PET data were preprocessed as follows according to the procedures described in our previous study [28]. The preprocessing of the volumetric MRI data was performed via the Voxel-Based Morphometry 8 (VBM8) Toolbox (http://dbm.neuro.uni-jena.de/vbm8), which involved two main segmentation and normalization steps. First, segmentation was performed on each MRI image to obtain the grey matter, white matter, and cerebrospinal fluid using adaptive maximum posterior and partial volume estimation [32, 33]. Two denoising methods, namely a spatially adaptive non-local means denoising filter and a classical Markov random field approach, were adopted to improve segmentation performance. Then, the grey matter images obtained from the segmentation step were used for the following analysis:

A diffeomorphic anatomical registration using exponential Lie algebra (DARTEL) protocol was applied to normalize the grey matter images [34] with iterative template creation and image registration, after which the grey matter maps were normalized to the Montreal Neurological Institute (MNI) space. The registered grey matter maps were multiplied by Jacobian determinants with only non-linear warping to exclude individual differences in total intracranial volume.

The FDG and florbetapir PET images of each subject were first co-registered to his/her MRI using a rigid body transformation, and subsequently were warped to the cohort-specific DARTEL template. Then, the standard uptake value ratio (SUVR) was calculated using the whole brain as the reference region for each FDG-PET and cerebellum as the reference region for each florbetapir PET.

The normalized grey matter images from MRI, SUVR images from FDG-PET, and SUVR images from florbetapir PET were then used for further analysis.

Feature extraction

After preprocessing, features needed to be extracted from each modality for the further prediction of MCI/pMCI with multi-modal and single-modality features. According to a prior anatomical automatic labeling (AAL) atlas [35], 90 regions of interest (ROIs) were defined (see Supplementary Table 2). Then, for each subject, 90 features were extracted for each modality. Specifically, for one ROI, the mean gray matter volume, the mean SUVR value of FDG-PET, and the mean SUVR value of florbetapir PET were calculated by averaging the corresponding value of all the voxels within that ROI as one feature for MRI, FDG-PET, and florbetapir PET, respectively. Thus each subject (i.e., each sample) had 90 features for each modality.

Prediction methods

Machine learning technologies such as sparse representation-based classification (SRC) use the given class labeling and sample information obtained from a training dataset to label new samples [36], it assumes that each test sample can be expressed as a sparse linear combination of the training samples, and class labels can be assigned via the minimum representation residual. In our recent study, SRC was extended to a multi-modal framework, named as weighted multi-modality sparse representation-based classification (wmSRC) for multi-modal neuroimaging data [28]. Here, wmSRC was used to distinguish MCI from NC and to predict pMCI among MCI. A description of the wmSRC method and the corresponding experimental settings are detailed below.

Table 2
The contributions from both types of PET images (FDG-PET and florbetapir PET) with all the 90 features from each modality

Modality	MCI versus NC			pMCI versus sMCI		
	ACC (%)	SE (%)	SP (%)	ACC (%)	SE (%)	SP (%)
florbetapir PET	70.5	67.3	73.5	63.7	64.4	63.0
FDG-PET	71.8	64.6	78.6	67.0	67.4	66.7
MRI	68.7	63.6	73.5	50.6	47.8	53.3
MRI + florbetapir PET	72.3	66.4	77.8	64.3	65.9	62.6
MRI + FDG-PET	73.1	62.7	82.9	70.6	71.1	70.0

MCI, mild cognitive impairment; NC, normal control; pMCI, progressive MCI; sMCI, stable MCI; ACC, classification accuracy; SE, classification sensitivity; SP, classification specificity.

Weighted multi-modality sparse representation-based classification (wmSRC)

Suppose there are N training samples from K classes and each sample includes M modalities. $A^m = \left[A_1^m, ..., A_l^m ..., A_K^m\right] \in \Re^{D\times N}$ denotes the m-th modality of the training samples, where D is the number of features, $N = N_1 + ... + N_l ... + N_K$, and $A_l^m = \left[a_1^{ml}, ..., a_i^{ml}, ...a_{N_l}^{ml}\right] \in \Re^{D\times N_l}$ consists of N_l training samples from the m-th modality of the l-th class. So, for a test sample y, the sparse coding can be calculated for each modality as:

$$x^m = \arg\min \left\|x^m\right\|_1, subject\ to \left\|A^m x^m - y^m\right\|_2 \le \varepsilon, m = 1, ..., M, \quad (1)$$

where $\|.\|_1$ represents the standard L1 norm, $\|.\|_2$ represents the standard Euclidean norm, $\varepsilon > 0$ is the error tolerance, $y^m \in \Re^D$ is the m-th modality of the test sample y, and $x^m = \left[x_1^m, ..., x_l^m, ..., x_K^m\right] \in \Re^N$ is the coding coefficient, where x_l^m consists of N_l representation coefficients that correspond to the m-th modality of the l-th class.

Then, the residual from the m-th modality of the l-th class can be denoted as:

$$r_l^m(y) = \left\|A^m x_l^m - y^m\right\|_2, m = 1, ..., M; l = 1, ..., K \quad (2)$$

Finally, the class label for the test sample y will be:

$$label\,(y) = arg\ min_l \sum_{m=1}^{M} \alpha_m r_l^m\,(y) \qquad (3)$$

where $\alpha_m \geq 0$ is the combining weight for the m-th modality, and α_m is constrained by $\sum_{m=1}^{M} \alpha_m = 1$.

Experimental settings

The convex problems in equation (1) can be efficiently optimized by a number of existing packages, such as L1-magic [37], the GPSR package [38], and the L1-homotopy package [39]. The GPSR package was used in this study.

Following the practices of a previous study by Zhang et al. [24], 10-fold cross-validation was repeated 10 times to avoid the bias generated in the classification step, and a grid search approach on each training set was implemented to optimize the combining weight parameters α. For each 10-fold cross-validation, the procedures were as follows. First, 10 subsets were randomly equally partitioned from the whole samples. Each time one subset was taken as the test set and the remaining nine were used as the training set. Then, weight selection was performed based on the training set with another 10-fold cross validation. In particular, a grid search approach with a range of [0, 1] at a step size of 0.1 was adopted to determine the weight parameters α of multiple modalities at each fold. Finally, the optimal weights were determined as the average of the weights obtained by the weight-selection process.

After determining the optimal value of weights α, the class labels for the test samples were assigned according to equations (1), (2), and (3). The performance of wmSRC was evaluated by calculating the accuracy, sensitivity, and specificity for the test samples. Accuracy was the proportion of samples that were correctly classified over all test samples; sensitivity was the proportion of positive-class samples that were correctly diagnosed; while specificity was the proportion of negative-class samples that were accurately identified. The final accuracy, sensitivity, and specificity were calculated by averaging the above cross-validation results.

Feature ranking

To find a small set of effective biomarkers that had good predictive power for MCI and pMCI, the 90 features from each modality were ranked based on the magnitude of the type-I error from the two-sample t-test, as described below. The feature ranking was performed on the training set from each fold of the 10-fold cross-validation. Specifically, for MRI, FDG-PET, and florbetapir PET, a two-sample t-test between MCI and NC, as well as between pMCI and sMCI was first performed on each feature of the training samples to obtain the corresponding discriminative p-value (type-I error). Then, all 90 features were ranked according to their p-value. These ranked features were used for the prediction of MCI versus pMCI.

MCI and pMCI prediction

The wmSRC method described above was adopted here to discriminate MCI from NC and to predict pMCI from sMCI. The prediction results were evaluated by calculating the averaged accuracy, sensitivity, and specificity from the cross-validations. Accuracy was the proportion of MCI + NC or pMCI + sMCI that were correctly predicted over all test samples, sensitivity was the proportion of MCI or pMCI that were correctly diagnosed, while specificity was the proportion of NC or sMCI that were accurately identified.

Contributions from both types of PET images

Different types of PET images, including FDG-PET and florbetapir PET, are always used for the diagnosis of MCI. Do they make different contributions to the prediction of MCI versus pMCI? Answering this question is important, so as to choose modalities that enhance predictions. In this study, all 90 features from each modality were used in the wmSRC method [28] for the discrimination of MCI from NC and prediction of pMCI versus sMCI. We used the single-modality features from FDG-PET, florbetapir PET, and MRI, and combinations of features from two modalities: MRI + FDG-PET and MRI + florbetapir PET.

Sensitive biomarkers from each modality

Ninety features were extracted from each modality (MRI, FDG-PET, and florbetapir PET) for the prediction of MCI and pMCI. A key issue was identifying which features were most sensitive in their predictive power. Therefore, wmSRC for three modalities (MRI + FDG-PET + florbetapir PET) and each single-modality (MRI, FDG-PET, and

florbetapir PET) was investigated using a different number (from 1 to 90) of the ranked features from each modality. Then, a small set of discriminating features was chosen from each modality to generate the final predictions.

RESULTS

Contribution from both types of PET images

The results from the florbetapir PET, FDG-PET, MRI, MRI + florbetapir PET, and MRI + FDG-PET based on all 90 features from each modality are shown in Table 2, which illustrates the contribution of the two PET modalities to the prediction of MCI versus pMCI. Of the single-modality predictions, florbetapir PET achieved an accuracy of 70.5% in predicting MCI and 63.7% in predicting pMCI, whereas FDG-PET achieved an accuracy of 71.8% in predicting MCI (1.3% higher than florbetapir PET) and 67.0% in predicting pMCI (3.3% higher than florbetapir PET).

Of the two-modality predictions, which combined the different types of PET with MRI, the combination of MRI + florbetapir PET achieved an accuracy of 72.3% in predicting MCI (3.6% higher than MRI alone), whereas prediction of pMCI occurred with an accuracy of 64.3% (13.7% higher than MRI only). The combination of MRI + FDG-PET achieved an accuracy of 73.1% in predicting MCI (4.4% higher than MRI alone and 0.8% higher than MRI + florbetapir PET) and 70.6% accuracy in predicting pMCI (20.0% higher than MRI alone and 6.3% higher than MRI + florbetapir PET).

The weights α in wmSRC that were optimized by the grid search approach for discriminating MCI from NC were 0.4 for MRI and 0.6 for FDG-PET for MRI + FDG-PET, and 0.4 for MRI and 0.6 for florbetapir PET for MRI + florbetapir PET. For discriminating pMCI from sMCI, the weights α were 0.2 for MRI and 0.8 for FDG-PET for MRI + FDG-PET, and 0.4 for MRI and 0.6 for florbetapir PET for MRI + florbetapir PET.

Sensitive biomarkers from each modality

To choose the top few sensitive biomarkers from each modality for the prediction of MCI and pMCI, we investigated different number (from 1 to 90) of ranked features for multi-modal discriminations (MRI + FDG-PET + florbetapir PET) and the single-modality discriminations (MRI, FDG-PET, and florbetapir PET). Subsequently, a small set of features from each modality were chosen for the final prediction, according to their predictive power.

The results from single-modality (MRI, FDG-PET, and florbetapir PET) and multi-modal (MRI + FDG-PET + florbetapir PET) analyses are displayed in Fig. 1. Figure 1a and 1b indicate that discriminating MCI from pMCI by combining features from multiple modalities was superior to single-modality features, and the single-modality results from FDG-PET were superior to those of florbetapir PET along with different number of the ranked features. In particular, the weights α in wmSRC for MRI + FDG-PET + florbetapir PET were optimized by a grid search approach and finally set as 0.4, 0.3, and 0.3 for MRI, FDG-PET, and florbetapir PET, respectively, for discriminating MCI from NC; and 0.1, 0.3, and 0.6, respectively, for discriminating pMCI from sMCI.

The multi-modal analysis achieved reasonable accuracy for discriminating MCI from pMCI even with a combination of only the top 6% (i.e., 6) features from each modality (MRI, FDG-PET, and florbetapir PET). Thus, to provide a conveniently small set of features to effectively predict MCI and pMCI, the top 6% of ranked features from each modality were chosen as sensitive biomarkers to obtain the final prediction.

Table 3 lists the most sensitive 6% of biomarkers from each modality and Fig. 2 shows them in the template space. Table 4 displays the prediction results from multi-modal (MRI + FDG-PET + florbetapir PET) and single-modality (MRI, FDG-PET, and florbetapir PET) analyses using the sensitive biomarkers shown in Table 3, as well as with all 90 features. For the discrimination of MCI from NC with the sensitive biomarkers, the multi-modal analysis achieved an accuracy of 76.7%, which was superior to single-modality analyses (MRI: 63.9%, florbetapir PET: 68.7%, FDG-PET: 73.6%). With all 90 features, the multi-modal analysis achieved an accuracy of 74.5%, which was superior to single-modality analyses (MRI: 68.7%, florbetapir PET: 70.5%, FDG-PET: 71.8%). These results show that when using the sensitive biomarkers, the discrimination performance for MCI versus NC was comparable to using all 90 features. For the discrimination of pMCI from sMCI, the combination of multi-modal sensitive biomarkers achieved an accuracy of 82.5%, which was superior to MRI (57.6%), florbetapir PET (73.2%), and FDG-PET (75.6%). The combination of all 90 multi-modal features achieved an accuracy of 77.8%, which was superior to MRI (50.6%), florbetapir PET (63.7%), and FDG-PET (67.0%). These

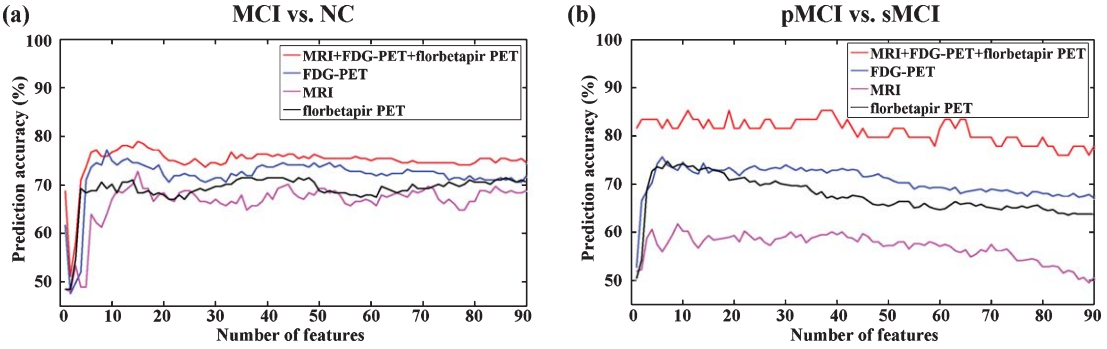

Fig. 1. The prediction accuracy from multi-modal (MRI + FDG-PET + florbetapir PET) and single-modality (MRI, FDG-PET, and florbetapir PET) analyses along with different number of the ranked features. (a) MCI versus NC and (b) pMCI versus sMCI.

Table 3
The sensitive biomarkers from each modality for predicting MCI and pMCI

	MCI versus NC		
No.	MRI	FDG-PET	florbetapir PET
1	left Hippocampus	left Posterior Cingulum	left Hippocampus
2	right Hippocampus	left Angular	right Hippocampus
3	left Amygdala	right Posterior Cingulum	right Posterior Cingulum
4	right Amygdala	left Postcentral	left Rectus
5	left Middle Temporal	left Precentral	right ParaHippocampal
6	left Inferior Temporal	left Paracentral lobule	left ParaHippocampal
	pMCI versus sMCI		
No.	MRI	FDG-PET	florbetapir PET
1	left Calcarine	left Posterior Cingulum	left Amygdala
2	left Cuneus	right Precentral	right Amygdala
3	right Middle Temporal (Polo part)	right Postcentral	left Putamen
4	right Cuneus	right Posterior Cingulum	right Putamen
5	left Middle Temporal (Polo part)	right Superior Parietal	left Superior Frontal
6	left Inferior Temporal	left Middle Temporal	right Thalamus

MCI, mild cognitive impairment; NC, normal control; pMCI, progressive MCI; sMCI, stable MCI.

results show that discriminating pMCI from sMCI using the sensitive biomarkers achieved better performance than using all 90 features.

Table 3 and Fig. 2 show that for the prediction of MCI, the hippocampus, amygdala, middle temporal, and inferior temporal regions may be significant biomarkers for MRI; the posterior cingulum gyrus, angular gyrus, precentral gyrus, postcentral gyrus, and paracentral lobule may be important for the FDG-PET modality; the hippocampus, posterior cingulum gyrus, and parahippocampal region may be crucial for the florbetapir PET modality. For the discrimination of pMCI from sMCI, the middle temporal, cuneus, and inferior temporal regions may be significant biomarkers for the MRI modality; posterior cingulum gyrus, precentral gyrus, postcentral gyrus, superior parietal, and middle temporal regions may be important for the FDG-PET modality; amygdala, putamen, superior frontal region, and thalamus may be crucial for the florbetapir PET modality.

DISCUSSION

In this paper, effective biomarkers for predicting MCI conversion were constructed by combining three modalities: MRI, FDG-PET, and florbetapir PET. The results showed that multi-modal predictions were superior to those from a single-modality. Furthermore, the results suggested that FDG-PET may contribute more to the accurate prediction of MCI and pMCI than florbetapir PET. Sensitive biomarkers for modality-specific brain regions were identified so as to enable effective and convenient prediction of MCI and pMCI.

FDG-PET and florbetapir PET

Two different types of PET images, which measure separately the metabolic or pathological burden of the brain, are always employed in disease diagnosis [15, 17, 19]. Thus, it is interesting to explore their contributions to predictions of MCI versus pMCI.

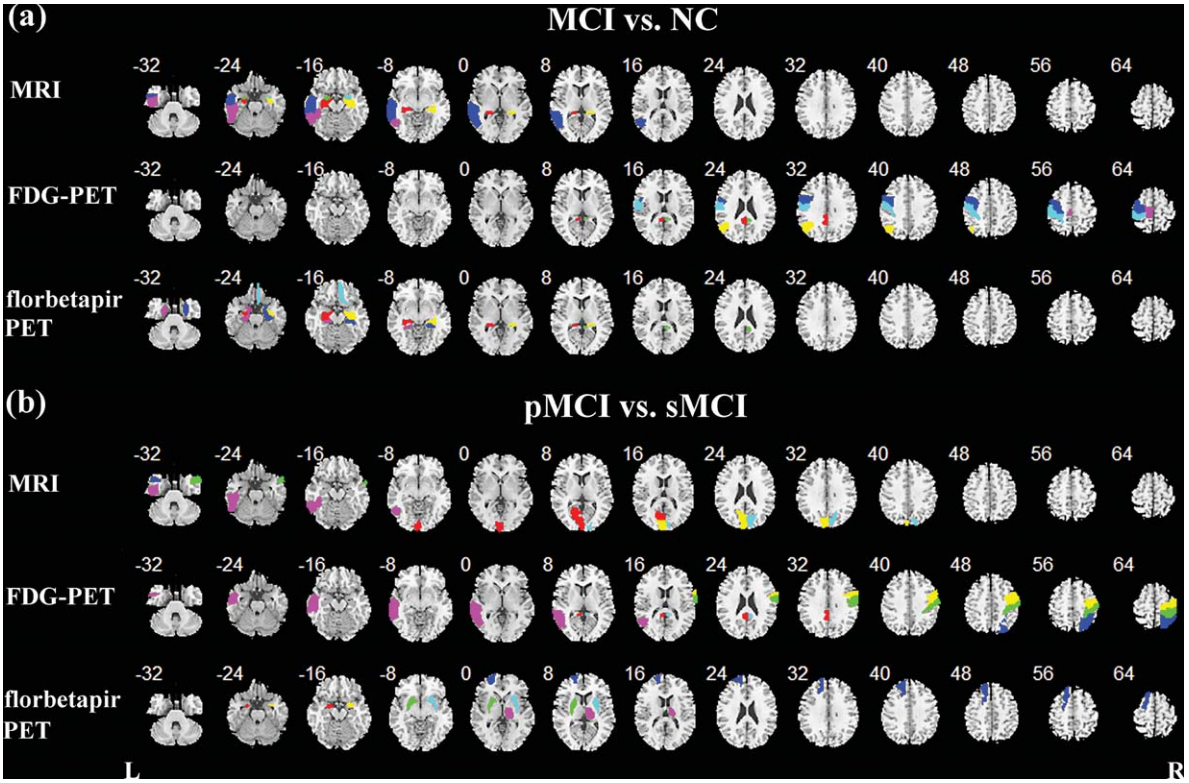

Fig. 2. The sensitive biomarkers from each modality for the prediction of (a) MCI and (b) pMCI. Each color in the figure denotes one biomarker.

Table 4
The performance for predicting MCI and pMCI with sensitive biomarkers as well as with all the 90 features

Methods	Sensitive biomarkers						90 features					
	MCI versus NC			pMCI versus sMCI			MCI versus NC			pMCI versus sMCI		
	ACC (%)	SE (%)	SP (%)	ACC (%)	SE (%)	SP (%)	ACC (%)	SE (%)	SP (%)	ACC (%)	SE (%)	SP (%)
MRI	63.9	50.9	75.7	57.6	50.4	64.8	68.7	63.6	73.5	50.6	47.8	53.3
florbetapir PET	68.7	66.4	70.9	73.2	79.6	66.7	70.5	67.3	73.5	63.7	64.4	63.0
FDG-PET	73.6	62.7	83.8	75.6	70.0	81.1	71.8	64.6	78.6	67.0	67.4	66.7
MRI+florbetapir PET + FDG-PET	76.7	63.6	89.7	82.5	81.5	83.5	74.5	66.4	82.1	77.8	74.1	81.5

MCI, mild cognitive impairment; NC, normal control; pMCI, progressive MCI; sMCI, stable MCI; ACC, classification accuracy; SE, classification sensitivity; SP, classification specificity.

Table 2 shows that with only the single-modality data, FDG-PET achieved better performance for discrimination of MCI versus pMCI than florbetapir PET. In combination with MRI, FDG-PET or florbetapir PET improved prediction performance over that obtained with MRI, FDG-PET, or florbetapir PET alone. The weights for MRI + FDG-PET and MRI + florbetapir PET were optimized by a grid search approach. For discriminating MCI from NC, weights were set at 0.4 for MRI and 0.6 for FDG-PET for MRI + FDG-PET and 0.4 for MRI and 0.6 for florbetapir PET for MRI + florbetapir PET. For discriminating pMCI from sMCI, weights were 0.2 for MRI and 0.8 for FDG-PET for MRI + FDG-PET, and 0.4 for MRI and 0.6 for florbetapir PET for MRI + florbetapir PET. These weights suggest that combining structural (i.e., MRI) and functional information (i.e., FDG-PET, florbetapir PET) improves the discrimination of MCI/pMCI. Further, the unequal weights imply differential contributions when combining modalities. In addition, for combinations involving MRI, FDG-PET provides more benefit for accurate discrimination of MCI/pMCI than florbetapir PET. This may because at the region-level (i.e., explorations of different brain regions), FDG-PET may offer more information than florbetapir PET [40].

Sensitive biomarkers

To choose sensitive biomarkers for the discrimination of MCI from pMCI, multi-modal (MRI + FDG-PET + florbetapir PET) and single-modality (MRI, FDG-PET, and florbetapir PET) analyses were performed using a different number of the ranked features (from 1 to 90) from each modality. The multi-modal analysis achieved better accuracy in discriminating MCI from NC and predicting pMCI or sMCI regardless of the number of ranked features used. Moreover, Fig. 1a and 1b make clear that, for the prediction of MCI/pMCI, the multi-modal results were far superior to the single-modality results with MRI, but only slightly better than those with florbetapir PET and FDG-PET, which further indicates that functional abnormalities in the brain may provide more helpful information for the prediction of MCI/pMCI than structural changes. When combining the three modalities (MRI + FDG-PET + florbetapir PET) in discriminating MCI from NC, the weight parameters optimized by a grid search approach were set to 0.4, 0.3, and 0.3 for MRI, FDG-PET, and florbetapir PET, respectively. When discriminating pMCI and sMCI in, the parameters were 0.1, 0.3, and 0.6, respectively. This suggests that the three modalities contribute differently, depending on the specific prediction, and may provide complementary contributions to the discrimination/prediction. In short, the combination of multi-modal information boosts the performance of discriminating MCI/pMCI, which has been reported in previous studies [20, 24]. Using a random forest classifier to combine MRI, CSF, and FDG-PET biomarkers, Gray et al. [20] achieved an accuracy of 74.6% in discriminating MCI from NC, which was better performance than single-modality biomarkers (67.3% for MRI, 61.7% for CSF, and 53.5% for FDG-PET). In [24], Zhang and colleagues used a multi-kernel support vector machine (mkSVM) to classify cases as MCI or NC. They found that combining MRI, CSF, and FDG-PET biomarkers achieved an accuracy of 76.4%, while the single-modality biomarkers attained accuracies of 72.0% (MRI), 71.4% (CSF), and 71.6% (FDG-PET). All these studies showed the effectiveness of combining biomarkers from multiple modalities.

Table 4 and Fig. 3 show that for the prediction of MCI and pMCI, a small set of sensitive biomarkers (the top 6% of ranked features) could achieve comparable or even better prediction performance than using all 90 features. Such a phenomenon may suggest that the complete set of brain regions (i.e., all 90 features) includes redundant information, and using all features may be not helpful and may interfere with the prediction process. Thus, selecting a small set of sensitive biomarkers may be necessary to make predictions more effective.

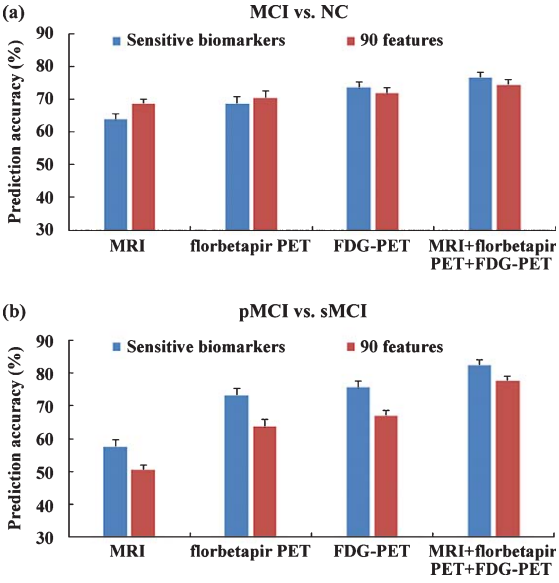

Fig. 3. The prediction accuracy for (a) MCI and (b) pMCI with sensitive biomarkers as well as with all the 90 features.

As shown in Table 3 and Fig. 2, sensitive biomarkers were identified for predicting MCI and pMCI. The middle temporal and inferior temporal regions for MRI, and the posterior cingulum, precentral, and postcentral regions for FDG-PET were shown to be biomarkers for MCI and pMCI, indicating that changes in these regions may occur primarily in the progressive stage but not in the early (or stable) stage of MCI, consistent with findings in previous studies [7, 17, 41–44]. Additionally, several biomarkers facilitated discrimination of MCI from NC but not pMCI from sMCI, such as the hippocampus and amygdala for MRI, the angular and paracentral lobule for FDG-PET, and the hippocampus, posterior cingulum gyrus, and parahippocampal region for florbetapir PET. This indicates that these changes may occur during the progressive as well as the stable stage of MCI. Furthermore, several other biomarkers may be helpful for the recognition of pMCI, including the cuneus for MRI, the superior parietal and middle temporal lobes for FDG-PET, and the amygdala, putamen, superior frontal region, and thalamus for florbetapir PET. Many of these biomarkers have been indicated as significant in MCI patients in previous studies [10, 17, 43, 45–50], and combining these biomark-

ers could achieve effective predictions for MCI and pMCI patients.

Despite these encouraging results, this study has some limitations. First, only three imaging modalities were investigated. Studies have indicated that imaging data or information from other sources, such as CSF, are also effective biomarkers for MCI prediction. The current study was limited to MRI, FDG-PET, and florbetapir PET because not all participants had information from other modalities available. Second, the modality-specific biomarkers for MCI/pMCI obtained in this paper were only based on the significance of the *p*-value obtained from the two-sample *t*-tests; other feature selection methods should be considered in future work.

Conclusion

For predicting MCI/pMCI converters, the current study identified several modality-specific sensitive biomarkers, such as the hippocampus, amygdala, middle temporal, and inferior temporal lobes for MRI, the posterior cingulum, precentral, and postcentral regions for FDG-PET, and the hippocampus, amygdala, and putamen for florbetapir PET. Combining these modality-specific biomarkers achieved satisfactory prediction results for MCI/pMCI. Further, the results suggested that FDG-PET may contribute more to accurate prediction of MCI/pMCI than florbetapir PET in region-level analyses. These results offer new insights into our understanding of patients with MCI/pMCI and may be important for the accurate and timely diagnosis of MCI/pMCI; future studies could usefully explore further these findings.

ACKNOWLEDGMENTS

This work is supported by the 863 Program (2015AA020912), the Funds for International Cooperation and Exchange of the National Natural Science Foundation of China (61210001), the General Program of National Natural Science Foundation of China (61571047) and the Fundamental Research Funds for the Central Universities.

Data collection and sharing for this project was funded by the Alzheimer's Disease Neuroimaging Initiative (ADNI) (National Institutes of Health Grant U01 AG024904) and DOD ADNI (Department of Defense award number W81XWH-12-2-0012). ADNI is funded by the National Institute on Aging, the National Institute of Biomedical Imaging and Bioengineering, and through generous contributions from the following: AbbVie, Alzheimer's Association; Alzheimer's Drug Discovery Foundation; Araclon Biotech; BioClinica, Inc.; Biogen; Bristol-Myers Squibb Company; CereSpir, Inc.; Eisai Inc.; Elan Pharmaceuticals, Inc.; Eli Lilly and Company; EuroImmun; F. Hoffmann-La Roche Ltd and its affiliated company Genentech, Inc.; Fujirebio; GE Healthcare; IXICO Ltd.; Janssen Alzheimer Immunotherapy Research & Development, LLC.; Johnson & Johnson Pharmaceutical Research & Development LLC.; Lumosity; Lundbeck; Merck & Co., Inc.; Meso Scale Diagnostics, LLC.; NeuroRx Research; Neurotrack Technologies; Novartis Pharmaceuticals Corporation; Pfizer Inc.; Piramal Imaging; Servier; Takeda Pharmaceutical Company; and Transition Therapeutics. The Canadian Institutes of Health Research is providing funds to support ADNI clinical sites in Canada. Private sector contributions are facilitated by the Foundation for the National Institutes of Health (http://www.fnih.org). The grantee organization is the Northern California Institute for Research and Education, and the study is coordinated by the Alzheimer's Disease Cooperative Study at the University of California, San Diego. ADNI data are disseminated by the Laboratory for Neuro Imaging at the University of Southern California.

Authors' disclosures available online (http://j-alz.com/manuscript-disclosures/15-1010r1).

SUPPLEMENTARY MATERIAL

The supplementary material is available in the electronic version of this article: http://dx.doi.org/10.3233/JAD-151010.

REFERENCES

[1] Grundman M, Petersen RC, Ferris SH, Thomas RG, Aisen PS, Bennett DA, Foster NL, Jack CR Jr, Galasko DR, Doody R (2004) Mild cognitive impairment can be distinguished from Alzheimer disease and normal aging for clinical trials. *Arch Neurol* **61**, 59-66.

[2] Petersen RC, Smith GE, Waring SC, Ivnik RJ, Tangalos EG, Kokmen E (1999) Mild cognitive impairment: Clinical characterization and outcome. *Arch Neurol* **56**, 303-308.

[3] Tang X, Holland D, Dale AM, Younes L, Miller MI (2015) Baseline shape diffeomorphometry patterns of subcortical and ventricular structures in predicting conversion of mild cognitive impairment to Alzheimer's disease. *J Alzheimers Dis* **44**, 599-611.

[4] McKhann G, Drachman D, Folstein M, Katzman R, Price D, Stadlan EM (1984) Clinical diagnosis of Alzheimer's disease Report of the NINCDS-ADRDA Work Group* under

the auspices of Department of Health and Human Services Task Force on Alzheimer's Disease. *Neurology* **34**, 939-939.

[5] Westman E, Muehlboeck J-S, Simmons A (2012) Combining MRI and CSF measures for classification of Alzheimer's disease and prediction of mild cognitive impairment conversion. *Neuroimage* **62**, 229-238.

[6] Westman E, Simmons A, Zhang Y, Muehlboeck J-S, Tunnard C, Liu Y, Collins L, Evans A, Mecocci P, Vellas B (2011) Multivariate analysis of MRI data for Alzheimer's disease, mild cognitive impairment and healthy controls. *Neuroimage* **54**, 1178-1187.

[7] Whitwell JL, Shiung MM, Przybelski S, Weigand SD, Knopman DS, Boeve BF, Petersen RC, Jack C (2008) MRI patterns of atrophy associated with progression to AD in amnestic mild cognitive impairment. *Neurology* **70**, 512-520.

[8] Ewers M, Walsh C, Trojanowski JQ, Shaw LM, Petersen RC, Jack CR, Feldman HH, Bokde AL, Alexander GE, Scheltens P (2012) Prediction of conversion from mild cognitive impairment to Alzheimer's disease dementia based upon biomarkers and neuropsychological test performance. *Neurobiol Aging* **33**, 1203-1214.

[9] Jefferson AL, Gifford KA, Damon S, Chapman IV, Liu GW, Sparling D, Dobromyslin J, Salat V, Alzheimer's Disease Neuroimaging D, Initiative (2014) Gray & white matter tissue contrast differentiates Mild Cognitive Impairment converters from non-converters. *Brain Imaging Behav* **9**, 141-148.

[10] Fan Y, Batmanghelich N, Clark CM, Davatzikos C, Alzheimer's Disease Neuroimaging, Initiative (2008) Spatial patterns of brain atrophy in MCI patients, identified via high-dimensional pattern classification, predict subsequent cognitive decline. *Neuroimage* **39**, 1731-1743.

[11] Zhang Y, Schuff N, Camacho M, Chao LL, Fletcher TP, Yaffe K, Woolley SC, Madison C, Rosen HJ, Miller BL (2013) MRI markers for mild cognitive impairment: Comparisons between white matter integrity and gray matter volume measurements. *PloS One* **8**, e66367.

[12] Willette AA, Calhoun VD, Egan JM, Kapogiannis D, Alzheimer's Disease Neuroimaging, Initiative (2014) Prognostic classification of mild cognitive impairment and Alzheimer's disease: MRI independent component analysis. *Psychiatry Res* **224**, 81-88.

[13] Risacher SL, Saykin AJ, West JD, Shen L, Firpi HA, McDonald BC, Alzheimer's Disease Neuroimaging, Initiative (2009) Baseline MRI predictors of conversion from MCI to probable AD in the ADNI cohort. *Curr Alzheimer Res* **6**, 347-361.

[14] Mosconi L, Perani D, Sorbi S, Herholz K, Nacmias B, Holthoff V, Salmon E, Baron J-C, De Cristofaro M, Padovani A (2004) MCI conversion to dementia and the APOE genotype A prediction study with FDG-PET. *Neurology* **63**, 2332-2340.

[15] Chen K, Ayutyanont N, Langbaum JB, Fleisher AS, Reschke C, Lee W, Liu X, Bandy D, Alexander GE, Thompson PM (2011) Characterizing Alzheimer's disease using a hypometabolic convergence index. *Neuroimage* **56**, 52-60.

[16] Cerami C, Della Rosa P, Magnani G, Marcone A, Cappa S, Perani D (2013) Heterogeneity of brain glucose metabolism in single subjects with mild cognitive impairment: The predictive role of [18F] FDG PET voxel-based imaging. *Neurology* **80**, 6-40.

[17] Camus V, Payoux P, Barré L, Desgranges B, Voisin T, Tauber C, La Joie R, Tafani M, Hommet C, Chételat G (2012) Using PET with 18F-AV-45 (florbetapir) to quantify brain amyloid load in a clinical environment. *Eur J Nucl Med Mol Imaging* **39**, 621-631.

[18] Rosenberg PB, Wong D, Edell S, Ross J, Joshi A, Brašić J, Zhou Y, Raymont V, Kumar A, Ravert H (2013) Cognition and amyloid load in Alzheimer disease imaged with florbetapir F 18 (AV-45) positron emission tomography. *Am J Geriatr Psychiatry* **21**, 272-278.

[19] Landau S, Harvey D, Madison C, Reiman E, Foster N, Aisen P, Petersen R, Shaw L, Trojanowski J, Jack C (2010) Comparing predictors of conversion and decline in mild cognitive impairment. *Neurology* **75**, 230-238.

[20] Gray KR, Aljabar P, Heckemann RA, Hammers A, Rueckert D, Alzheimer's Disease Neuroimaging, Initiative (2013) Random forest-based similarity measures for multi-modal classification of Alzheimer's disease. *Neuroimage* **65**, 167-175.

[21] Walhovd K, Fjell A, Dale A, McEvoy L, Brewer J, Karow D, Salmon D, Fennema-Notestine C, Alzheimer's Disease Neuroimaging Initiative (2010) Multi-modal imaging predicts memory performance in normal aging and cognitive decline. *Neurobiol Aging* **31**, 1107-1121.

[22] Zhang D, Shen D, Alzheimer's Disease Neuroimaging, Initiative (2012) Predicting future clinical changes of MCI patients using longitudinal and multimodal biomarkers. *PloS One* **7**, e33182.

[23] Liu Y, Wu X, Chen K, Yao L (2014) Combining multimodal neuroimaging biomarkers in the diagnosis of Alzheimer's disease and mild cognitive impairment. *Neurosci Biomed Eng* **2**, 159-165.

[24] Zhang D, Wang Y, Zhou L, Yuan H, Shen D, Alzheimer's Disease Neuroimaging, Initiative (2011) Multimodal classification of Alzheimer's disease and mild cognitive impairment. *Neuroimage* **55**, 856-867.

[25] Davatzikos C, Bhatt P, Shaw LM, Batmanghelich KN, Trojanowski JQ (2011) Prediction of MCI to AD conversion, via MRI, CSF biomarkers, and pattern classification. *Neurobiol Aging* **32**, 2322. e2319-2322. e2327.

[26] Vemuri P, Wiste H, Weigand S, Shaw L, Trojanowski J, Weiner M, Knopman D, Petersen R, Jack C (2009) MRI and CSF biomarkers in normal, MCI, and AD subjects predicting future clinical change. *Neurology* **73**, 294-301.

[27] Walhovd K, Fjell A, Brewer J, McEvoy L, Fennema-Notestine C, Hagler D, Jennings R, Karow D, Dale A (2010) Combining MR imaging, positron-emission tomography, and CSF biomarkers in the diagnosis and prognosis of Alzheimer disease. *Am J Neuroradiol* **31**, 347-354.

[28] Xu L, Wu X, Chen K, Yao L (2015) Multi-modality sparse representation-based classification for Alzheimer's disease and mild cognitive impairment. *Comput Methods Programs Biomed* **122**, 182-190.

[29] Folstein MF, Folstein SE, McHugh PR (1975) "Mini-mental state": A practical method for grading the cognitive state of patients for the clinician. *J Psychiatr Res* **12**, 189-198.

[30] Morris JC (1993) The Clinical Dementia Rating (CDR): Current version and scoring rules. *Neurology* **43**, 2412-2414.

[31] Wechsler D (1987) *Wechsler Memory Scale—Revised manual*. Psychological Corporation, San Antonio, TX.

[32] Rajapakse JC, Giedd JN, Rapoport JL (1997) Statistical approach to segmentation of single-channel cerebral MR images. *IEEE Trans Med Imaging* **16**, 176-186.

[33] Tohka J, Zijdenbos A, Evans A (2004) Fast and robust parameter estimation for statistical partial volume models in brain MRI. *Neuroimage* **23**, 84-97.

[34] Ashburner J (2007) A fast diffeomorphic image registration algorithm. *Neuroimage* **38**, 95-113.

[35] Tzourio-Mazoyer N, Landeau B, Papathanassiou D, Crivello F, Etard O, Delcroix N, Mazoyer B, Joliot M (2002) Automated anatomical labeling of activations in SPM using a macroscopic anatomical parcellation of the MNI MRI single-subject brain. *Neuroimage* **15**, 273-289.

[36] Wright J, Yang AY, Ganesh A, Sastry SS, Ma Y (2009) Robust face recognition via sparse representation. *IEEE Trans Pattern Anal Mach Intell* **31**, 210-227.

[37] Candes E, Romberg J. (2005) l1-magic: Recovery of sparse signals via convex programming, http://statweb. stanford.edu/ candes/l1magic/downloads/l1magic.pdf.

[38] Figueiredo MA, Nowak RD, Wright SJ (2007) Gradient projection for sparse reconstruction: Application to compressed sensing and other inverse problems. *IEEE J Sel Top Signal Process* **1**, 586-597.

[39] Asif MS, Romberg J. (2013) l1 Homotopy: A MATLAB toolbox for homotopy algorithms in l1 norm minimization problems, http://users.ece.gatech.edu/sasif/homotopy/.

[40] Bailly M, Ribeiro MJS, Vercouillie J, Hommet C, Gissot V, Camus V, Guilloteau D (2015) 18F-FDG and 18F-florbetapir PET in clinical practice: Regional analysis in mild cognitive impairment and Alzheimer disease. *Clin Nucl Med* **40**, e111-e116.

[41] Patterson JC, Lilien DL, Takalkar A, Pinkston JB (2010) Early detection of brain pathology suggestive of early AD using objective evaluation of FDG-PET scans. *Int J Alzheimers Dis* **2011**, pii:946590.

[42] Minoshima S, Giordani B, Berent S, Frey KA, Foster NL, Kuhl DE (1997) Metabolic reduction in the posterior cingulate cortex in very early Alzheimer's disease. *Ann Neurol* **42**, 85-97.

[43] Whitwell JL, Przybelski SA, Weigand SD, Knopman DS, Boeve BF, Petersen RC, Jack CR (2007) 3D maps from multiple MRI illustrate changing atrophy patterns as subjects progress from mild cognitive impairment to Alzheimer's disease. *Brain* **130**, 1777-1786.

[44] He W, Liu D, Radua J, Li G, Han B, Sun Z (2015) Meta-analytic comparison between PIB-PET and FDG-PET results in Alzheimer's disease and MCI. *Cell Biochem Biophysics* **71**, 17-26.

[45] Mosconi L (2005) Brain glucose metabolism in the early and specific diagnosis of Alzheimer's disease. *Eur J Nucl Med Mol Imaging* **32**, 486-510.

[46] Basso M, Yang J, Warren L, MacAvoy MG, Varma P, Bronen RA, van Dyck CH (2006) Volumetry of amygdala and hippocampus and memory performance in Alzheimer's disease. *Psychiatry Res* **146**, 251-261.

[47] Chen Y, Wolk D, Reddin J, Korczykowski M, Martinez P, Musiek E, Newberg A, Julin P, Arnold S, Greenberg J (2011) Voxel-level comparison of arterial spin-labeled perfusion MRI and FDG-PET in Alzheimer disease. *Neurology* **77**, 1977-1985.

[48] Cuingnet R, Gerardin E, Tessieras J, Auzias G, Lehéricy S, Habert M-O, Chupin M, Benali H, Colliot O, Initiative AsDN (2011) Automatic classification of patients with Alzheimer's disease from structural MRI: A comparison of ten methods using the ADNI database. *Neuroimage* **56**, 766-781.

[49] Sabuncu MR, Desikan RS, Sepulcre J, Yeo BTT, Liu H, Schmansky NJ, Reuter M, Weiner MW, Buckner RL, Sperling RA (2011) The dynamics of cortical and hippocampal atrophy in Alzheimer disease. *Arch Neurol* **68**, 1040-1048.

[50] Stoub TR, Dickerson BC (2014) Parahippocampal white matter volume predicts Alzheimer's disease risk in cognitively normal old adults. *Neurobiol Aging* **35**, 1855-1861.